Medical & Biological Engineering & Computing (2019) 57:519–532
https://doi.org/10.1007/s11517-018-1895-z

ORIGINAL ARTICLE

# Construction and evaluation of a model for wheelchair propulsion in an individual with tetraplegia

Brooke Odle[1,2,3] · Jeffrey Reinbolt[4] · Gail Forrest[2,5] · Trevor Dyson-Hudson[2,5]

Received: 17 March 2018 / Accepted: 5 September 2018 / Published online: 25 September 2018


## Abstract

Upper limb overuse injuries are common in manual wheelchair users with spinal cord injury. Patient-specific in silico models enhance experimental biomechanical analyses by estimating in vivo shoulder muscle and joint contact forces. Current models exclude deep shoulder muscles that have important roles in wheelchair propulsion. Freely accessible patient-specific models have not been generated for persons with tetraplegia, who have a greater risk for shoulder pain and injury. The objectives of this work were to (i) construct a freely accessible, in silico, musculoskeletal model capable of generating patient-specific dynamic simulations of wheelchair propulsion and (ii) establish proof-of-concept with data obtained from an individual with tetraplegia. Constructed with OpenSim, the model features muscles excluded in existing models. Shoulder muscle forces and activations were estimated via inverse dynamics. Mean absolute error of estimated muscle activations and fine-wire electromyography (EMG) recordings was computed. Mean muscle activation for five consecutive stroke cycles demonstrated good correlation (0.15–0.17) with fine-wire EMG. These findings, comparable to other studies, suggest that the model is capable of estimating shoulder muscle forces during wheelchair propulsion. The additional muscles may provide a greater understanding of shoulder muscle contribution to wheelchair propulsion. The model may ultimately serve as a powerful clinical tool.

**Keywords** Upper limb · Biomechanics · Musculoskeletal model · Wheelchair propulsion · Spinal cord injuries

## 1 Introduction

Repetitive strain injuries at the shoulder are among the most frequent causes of musculoskeletal pain and disability in manual wheelchair using individuals with spinal cord injury (SCI) [1–3]. Partial innervation and impaired balance of shoulder, scapular, and thoracohumeral muscles may place individuals with tetraplegia at higher risk for developing shoulder pain, especially during weight-bearing upper limb activities like wheelchair propulsion [4–9]. Researchers have investigated the relationship between manual wheelchair propulsion and shoulder pain and injury, by exploring wheelchair setup optimization, wheelchair propulsion style, and wheelchair propulsion mechanics. However, these biomechanical studies were limited by the inability to measure in vivo joint contact forces in the absence of invasive means [10] and the lack of a direct minimally invasive method to measure muscle forces in vivo [11–14]. Instead, in vivo shoulder joint and muscle forces during wheelchair propulsion were estimated via computer graphics-based models.

Early models used for wheelchair propulsion simulations [15–19] were not patient-specific, so they could not be personalized to assess the effectiveness of a treatment, identify patients that can be treated with particular interventions, and predict which treatment should be performed on a patient and how it should be performed [20]. Dubowsky et al. [12] were the first to construct and validate a patient-specific model of wheelchair propulsion. Utilizing AnyBody software (AnyBody Technology A/S, Aalborg, Denmark), they investigated the

✉ Brooke Odle
bmo13@case.edu

1 Department of Biomedical Engineering, New Jersey Institute of Technology, 323 Martin Luther King Blvd, Newark, NJ 07102, USA

2 Kessler Foundation, 1199 Pleasant Valley Way, West Orange, NJ 07052, USA

3 Present address: Department of Biomedical Engineering, Case Western Reserve University, 10900 Euclid Avenue, Cleveland, OH 44106, USA

4 Department of Mechanical, Aerospace, and Biomedical Engineering, University of Tennessee, 1512 Middle Drive, Knoxville, TN 37996, USA

5 Department of Physical Medicine and Rehabilitation, Rutgers New Jersey Medical School, 185 South Orange Avenue, Newark, NJ 07101, USA

minimization of joint forces at the shoulder, aiming to address previous kinetic wheelchair propulsion studies that found high joint loading at the shoulder. Properties of the rigid-bone geometries and muscle geometries were included to account for patient specificity. Their model was not freely accessible to the research community, however, limiting collaboration, replication of results, and advancing the field [21–23].

When a published model is not available to address a specific research problem, researchers usually adapt a generic open-source musculoskeletal model [22]. Morrow et al. [24] utilized an inverse dynamics model, the open-source SIMM (Musculographics, Santa Rosa, CA) Stanford VA Model [25] and a custom optimization muscle model to determine shoulder joint contact forces during wheelchair activities. Rankin et al. [26, 27] also utilized the Stanford VA model to investigate upper limb demand and shoulder muscle contribution during wheelchair propulsion. However, the Stanford VA model is a kinematic model, so mass and segment inertia characteristics were required to generate dynamic simulations and determine shoulder muscle forces. Moreover, deep shoulder muscles, such as the serratus anterior, rhomboid major, and upper and middle trapezius, were not included in either model. Using fine-wire EMG, Mulroy et al. [7, 28] determined that both deep and superficial thoracohumeral muscles have important roles during wheelchair propulsion, and it is critical that these muscles be included in wheelchair propulsion applications. Also, despite having an open-source model as its foundation, Morrow and Rankin's adapted models were not freely available to the research community. Using the Stanford VA Model as the kinematic foundation, Saul et al. [22] published a dynamic upper limb model. Although this model is freely accessible and can be adapted to investigate specific research problems, including wheelchair propulsion biomechanics, it does not contain the deep thoracohumeral musculature.

We present the construction and evaluation of an open-source, computer graphics-based, patient-specific, musculoskeletal model of the shoulder that is capable of generating dynamic simulations of wheelchair propulsion (Wheelchair Propulsion Model). Specifically, the model estimates muscle force and activation during wheelchair propulsion. It includes previously unmodeled deep shoulder muscles, which also have a role in wheelchair propulsion. The model was constructed and evaluated with OpenSim [21, 29], an open-source modeling framework with patient-specific modeling capabilities for investigating dynamic simulations of movement. Previous simulation studies have either included individuals with paraplegia or a heterogeneous group of manual wheelchair users and the compared their findings with surface EMG. Given that they are at a higher risk for shoulder injuries, a patient-specific model that can be generated for manual wheelchair users with tetraplegia may be a powerful clinical tool. Thus, to establish proof of concept, the model was evaluated with fine-wire EMG data obtained from a manual wheelchair user with tetraplegia. This is the first wheelchair propulsion simulation study to incorporate fine-wire EMG data. Finally, this model as open source will be freely accessible to the OpenSim user community.

## 2 Materials and methods

### 2.1 Musculoskeletal model

A three-dimensional musculoskeletal model of the upper limb was constructed using OpenSim, an open-source musculoskeletal modeling and simulation framework for in silico investigations and exchange [29]. The Wheelchair Propulsion Model [30], based on the OpenSim distributed Arm 26 model, consisted of rigid bodies representing the spine and rib cage, clavicle, scapula, humerus, ulna, radius, and hand (Fig. 1). Body segment mass and inertia properties were obtained from cadaver studies [31]. The model has seven degrees of freedom representing the articulations at the shoulder, elbow, forearm, and wrist. The articulations at the shoulder are elevation plane, elevation angle, and rotation, while articulations at the elbow include elbow flexion and forearm rotation [30]. Shoulder elevation plane ranges from 0° to 180°. Shoulder elevation angle represents the thoracohumeral angle and ranges from 90° to 130° in the model. Although this range allows for full range of motion in the model, it should be noted that the

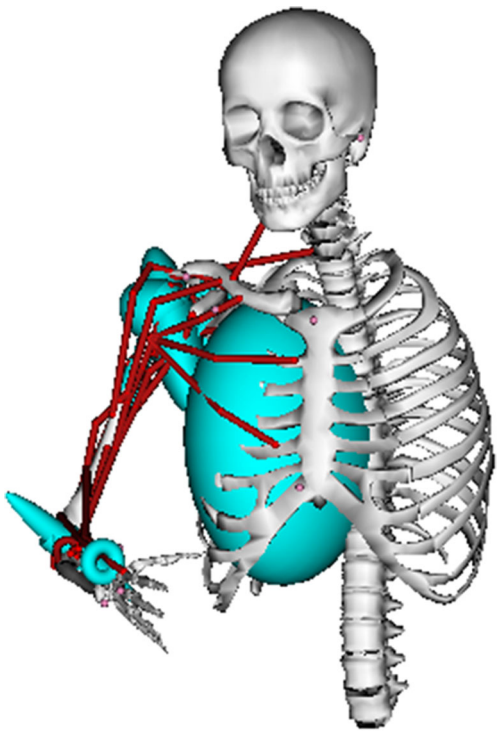

**Fig. 1** Wheelchair Propulsion Model with seven degrees of freedom, 26 musculotendon actuators, and wrapping objects

thoracohumeral angle of a manual wheelchair using patient with SCI will be a much smaller subset of this range. Shoulder rotation occurs about the long axis of the humerus and ranges from −90° (external rotation) to 90° (internal rotation). Elbow flexion is defined from 0° (full extension) to 130° (flexion). Forearm rotation is defined from −90° (supination) to 90° (pronation). The scapula and the clavicle move as a function of the humerus motion. The kinematics of the Wheelchair Propulsion Model is consistent with the Stanford VA Model [30]. The Model also rotates and translates about the *X-Y-Z* axes.

Thirty Hill-type musculotendon actuators were used to represent the muscles crossing the trunk, shoulder, elbow, and wrist [25, 32, 33]. The upper and middle trapezius muscles were added from the Head and Neck Model by Vasavada et al. [32]. The serratus anterior and rhomboid major were manually added to the model, according the design approach described by Holzbaur et al. [25]. Therefore, the serratus anterior was defined with one muscle path and three attachment points, while the rhomboid major was defined with one muscle path and two attachment points. All musculotendon actuator parameters (Table 1) were derived from previous published work [25, 32, 33]. The actuators were governed by muscle force-length-velocity relationships [34].

## 2.2 Experimental data collection and processing

To establish proof of concept, kinematic, kinetic, and fine wire muscle activation data collected during a wheelchair propulsion testing session [35] were implemented to evaluate the model's ability to estimate amplitude and timing of muscle forces for the shoulder complex muscles per stroke cycle. These data were collected from a 30-year-old male participant with chronic (duration of injury = 14 years) tetraplegia. The participant's neurological level of injury was C5 and motor level was C6 (*ASIA Impairment Scale [AIS] grade* A) [36]. His motor and sensory scores were not available at the time of data collection. His height and weight were 2 m and 79.1 kg, respectively. It is important to note that the experimental data were historical data, implemented in this proof-of-concept study in an effort to gain insight on how to design future experiments to refine the model.

For kinematic testing, reflective markers were placed bilaterally on each wheel and the bony landmarks of the upper limbs, trunk, and jaw. Marker placements were in accordance with the ISB recommendations [37], except for the markers placed on the T3 spinous process instead of the T8 spinous process and the lateral-superior border of the acromion instead of the glenohumeral joint rotation center. Markers were also placed on the right and left tempero-mandibular joints and the head of the third metacarpal joint. A passive marker motion capture system (M2 mcam cameras, Vicon Motion Systems, Oxford, UK) was used to collect three-dimensional positional data at 120 Hz. Post-processing of kinematic data entailed filtering with a fourth-order Butterworth low-pass filter with a 7-Hz cutoff frequency [35].

Kinetic data were collected using the Smart$^{WHEEL}$ (Out-Front, Mesa, AZ). These commercially available force and torque sensing pushrims were placed on both sides of the participant's wheelchair and the amplitude and direction of force applied to the pushrim during the push phase of the stroke cycle. These kinetic data were collected at 240 Hz and were synchronized to the kinematic and EMG data using an external trigger between the Smart$^{WHEEL}$ computer and the Vicon workstation. The test subject propelled his own wheelchair, at 2 mph, on a dynamometer that consisted of two independent steel tubular rollers (one for each wheel) using a four-belt tie-down system [35] (Fig. 2). Real-time speed feedback for maintaining speed was presented on a monitor in front of the roller system. Data collection for each trial lasted for 20 s and three trials were collected per test condition.

Muscle activation during the stroke cycle was determined using stainless steel nickel alloy insulated fine-wire electrodes (MA-300 EMG System, Motion Lab Systems, Inc., Baton Rouge, LA). Electrodes were inserted into 13 upper limb and trunk muscles: middle trapezius, upper trapezius, sternal pectoralis, rhomboid major, anterior, middle, and posterior deltoids, supraspinatus, infraspinatus, subscapularis, serratus anterior, biceps, and triceps. One pole of 13 preamplified electrodes was attached to the fine wires. The second pole was attached to Ag/AgCl surface electrodes placed over the surface of the muscle. The exception to this was the subscapularis because a second intramuscular needle electrode was attached. Data were collected at 2520 Hz with analog input to the Vicon workstation. Signals were low-pass filtered at 1250 Hz by the EMG collection unit (Motion Lab Systems, Inc., Baton Rouge, LA) and analog input to the Vicon workstation. EMG data were full wave rectified, and filtered using a fourth-order band-pass filter (20–150 Hz), and root-mean-square average with a 100-ms window was applied to create a linear envelope of the signal. The linear envelope was normalized to the mean amplitude of the greatest 1 s of muscle activity during a maximum voluntary contraction. Active EMG was defined as having an amplitude of greater than 5% of the maximum voluntary contraction for more than 5% of the stroke cycle [35].

Five consecutive right-sided push strokes were selected for analyses. Each stroke cycle was defined as the push phase followed by the recovery phase. For data processing purposes, the push phase began at the point when the moment about the axle exceeded two standard deviations above the resting amplitude. The recovery phase was defined as the period in between consecutive push phases, and began at the point at which the moment fell below the threshold set at two standard deviations above baseline. All kinematic, kinetic, and EMG data were normalized to 100% of the stroke cycle.

**Table 1** Muscle modeling parameters

| Muscle | Peak force (N) | Optimal fiber length (cm) | Tendon slack length (cm) |
|---|---|---|---|
| Shoulder | | | |
| Trapezius | | | |
| Upper | 78 | 8.4 | 12.0 |
| Middle | 377 | 9.2 | 7.3 |
| Serratus anterior | 677.3 | 17.5 | 0.3 |
| Rhomboid major | 217.1 | 17.9 | 0.5 |
| Deltoid | | | |
| Anterior | 1142.6 | 9.8 | 9.3 |
| Middle | 1142.6 | 10.8 | 11.0 |
| Posterior | 259.9 | 13.7 | 3.8 |
| Supraspinatus | 487.8 | 6.8 | 4.0 |
| Infraspinatus | 1210.8 | 7.6 | 3.1 |
| Subscapularis | 1377.8 | 8.7 | 3.3 |
| Teres minor | 354.3 | 7.4 | 7.1 |
| Teres major | 425.4 | 16.2 | 2.0 |
| Pectoralis major | | | |
| Clavicular | 364.4 | 14.4 | 0.3 |
| Sternal | 515.4 | 13.8 | 8.9 |
| Ribs | 390.5 | 13.8 | 13.2 |
| Latissimus dorsi | | | |
| Thoracic | 389.1 | 25.4 | 12.0 |
| Lumbar | 389.1 | 23.3 | 17.7 |
| Iliac | 281.7 | 27.9 | 14.0 |
| Coracobrachialis | 242.5 | 9.3 | 9.7 |
| Elbow | | | |
| Triceps | | | |
| Long | 798.5 | 13.4 | 12.0 |
| Lateral | 624.3 | 11.4 | 9.8 |
| Medial | 624.3 | 11.4 | 9.1 |
| Anconeus | 350.0 | 2.7 | 1.8 |
| Supinator | 476.0 | 3.3 | 2.8 |
| Biceps | | | |
| Long | 624.3 | 11.6 | 27.2 |
| Short | 435.6 | 13.2 | 19.2 |
| Brachialis | 987.3 | 8.6 | 5.4 |
| Brachioradialis | 261.3 | 17.3 | 13.3 |

## 2.3 Static optimization

Prior to generating static optimization simulations to estimate shoulder muscle forces during wheelchair propulsion, the anthropometry of the generic musculoskeletal model was scaled to match the height and weight of the subject. Virtual markers were placed on the generic model, in accordance with the experimental marker locations on the subject. The dimensions of each segment in the model were scaled so that the distances between the virtual markers matched the distances between the experimental markers. Body segment masses on the model were adjusted so that the total body mass was equivalent to the mass of the subject.

Upon generating the patient-specific model, inverse kinematics and dynamics simulations were subsequently generated. Static optimization was used to estimate the forces of the shoulder complex muscles during manual wheelchair propulsion. This inverse dynamics-based optimization technique resolved the computed net joint moments into individual muscle forces. This was accomplished by solving the equations of motion, but since there are more unknown muscles than equations, the problem was underdetermined. Optimization was used to address this redundancy, and minimization of the sum of muscle activations squared was selected as the objective function. Muscle activation is approximately equal to muscle stress multiplied by a

**Fig. 2** Experimental setup of the wheelchair propulsion study. Reflective markers were placed on the upper limb and trunk to track their position during the stroke cycle. Fine-wire electrodes were used to collect the muscle activity during the stroke cycle. Smart$^{WHEELS}$ were placed bilaterally on the wheelchair to record the force exerted by the hand to push rim during propulsion. The participant propelled his own wheelchair on a dynamometer

proportionality constant [34]. The selection of the objective function was in accordance with van der Helm [15], who suggested that the minimization of muscle stresses squared allowed for distribution of muscle forces based on muscle cross-sectional area and was computationally efficient. Outputs of the static optimization technique were estimated muscle activations and forces to generate the inverse dynamics joint moments.

### 2.4 Model validation

Currently, there is no technique that allows for the direct minimally invasive measurement of muscle forces in vivo [12–14]. As an alternative, a common and accepted method for evaluating muscle forces is to compare the estimated muscle activation patterns with experimental EMG activity patterns [38]. However, EMG cannot verify the magnitude of estimated muscle force [13, 38, 39]. To evaluate the estimated muscle forces with a quantitative approach addressing the magnitude of force, the mean absolute error (*MAE*), previously used to validate computer graphics-based models [12, 15, 33], was calculated for each muscle's activity envelope, using the following equations:

$$MAE = 1/n \sum_{i=1}^{n} |MA_i - EA_i|$$

where $n$ is the number of time frames within a propulsion cycle, $MA_i$ is the measured EMG muscle activity as a percentage of maximum voluntary contraction on frame $i$, and $EA_i$ is the model estimated muscle activity as a percentage of maximum muscle force on frame $i$. One assumption in utilizing this approach is that there is a linear relationship between EMG and muscle force [40]. An average *MAE* of less than 0.10 represents an excellent quantitative correlation, while a value between 0.10 and 0.20 represents a good correlation, and a value greater than 0.20 represents a poor correlation [12, 15]. This study was the first wheelchair propulsion simulation study to compare estimated muscle activity with experimental fine-wire EMG collected directly from the participant being investigated.

## 3 Results

### 3.1 Inverse kinematics and dynamics simulations

In order to generate dynamic simulations of wheelchair propulsion, the model was scaled to the participant's dimensions and inverse kinematics and dynamics simulations were generated. Inverse kinematics simulations were determined for shoulder elevation (Fig. 3, top panel), elevation angle (Fig. 3 middle panel), and shoulder rotation (Fig. 3, bottom panel) for all five stroke cycles. The modeled kinematics were very consistent across the stroke cycles for each shoulder articulation. The average peak shoulder elevation was 38.5° (±0.3°) during push phase and 37.2° (±1.0°) during the recovery phase. The average peak elevation angle was 13.9° (±10.1°) during push phase and 33° (±3.4°) during recovery for all the cycles analyzed. The average peak shoulder rotation was 56.6° (±0.9°) during push phase and 56.7° (±0.9°) during recovery. Inverse kinematics simulations were also generated for elbow flexion (Fig. 4, top panel) and forearm rotation (Fig. 4, bottom panel). The modeled elbow kinematics were also very consistent across all five stroke cycles. The average peak elbow flexion was 85.7° (±0.3°) during push phase and 67.9° (±6.8°) during recovery. The average peak forearm rotation was 85.7° (±2.3°) during push phase and 28.8° (±4.5°) during recovery. To validate the inverse kinematics solutions, the root-mean-squared error of the virtual markers on the model and the experimental marker were computed for each frame. The RMS for each frame, across all five stroke cycles, was less than 1 cm. The maximum allowance of error due to soft tissue artifact was 1 cm, as determined by Cereatti et al. [41] and Chiari et al. [42].

Inverse dynamics simulations were generated at the shoulder for all five stroke cycles. Of the three shoulder degrees of freedom, the average peak moment about the shoulder elevation plane was the greatest during the push phase (18.5 Nm ± 1.0 Nm) and the recovery phase (16 Nm ± 1.7 Nm). Peak shoulder elevation plane moment occurred during the push phase. The average peak moment responsible for shoulder elevation angle was greater during the recovery phase (1.4 Nm ± 0.7 Nm) than the push phase (− 4.6 Nm ± 0.9 Nm). Peak shoulder elevation angle moment occurred during the recovery phase. The average

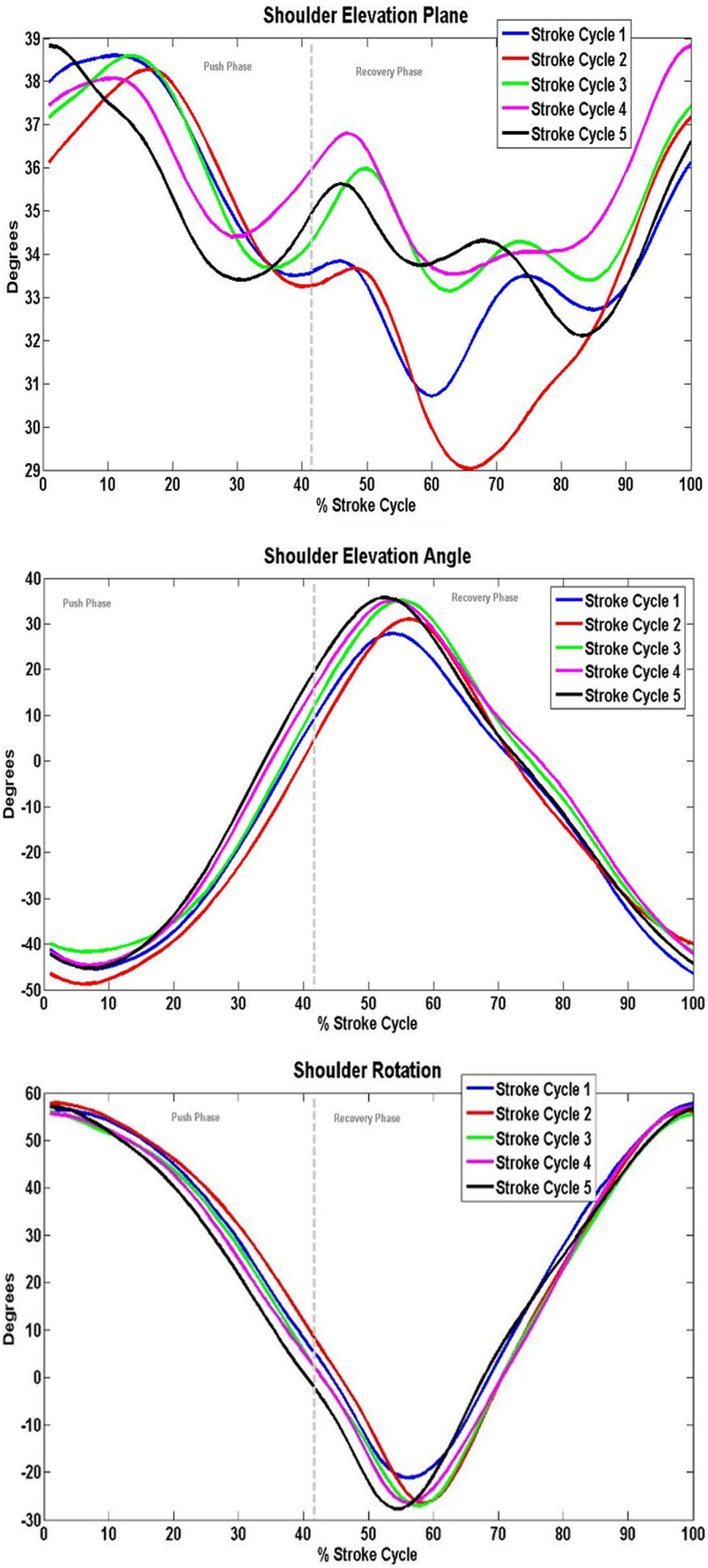


**Fig. 3** Kinematic profiles of the shoulder generated by inverse kinematics simulations for all five stroke cycles. Shoulder elevation plane angles are presented in the top panel, while shoulder elevation and shoulder rotation angles are presented in the middle and bottom panels, respectively. The transition from push phase to recovery phase is indicated by the dotted line, in each panel. All angles are measured in degrees and are presented for 100% stroke cycle

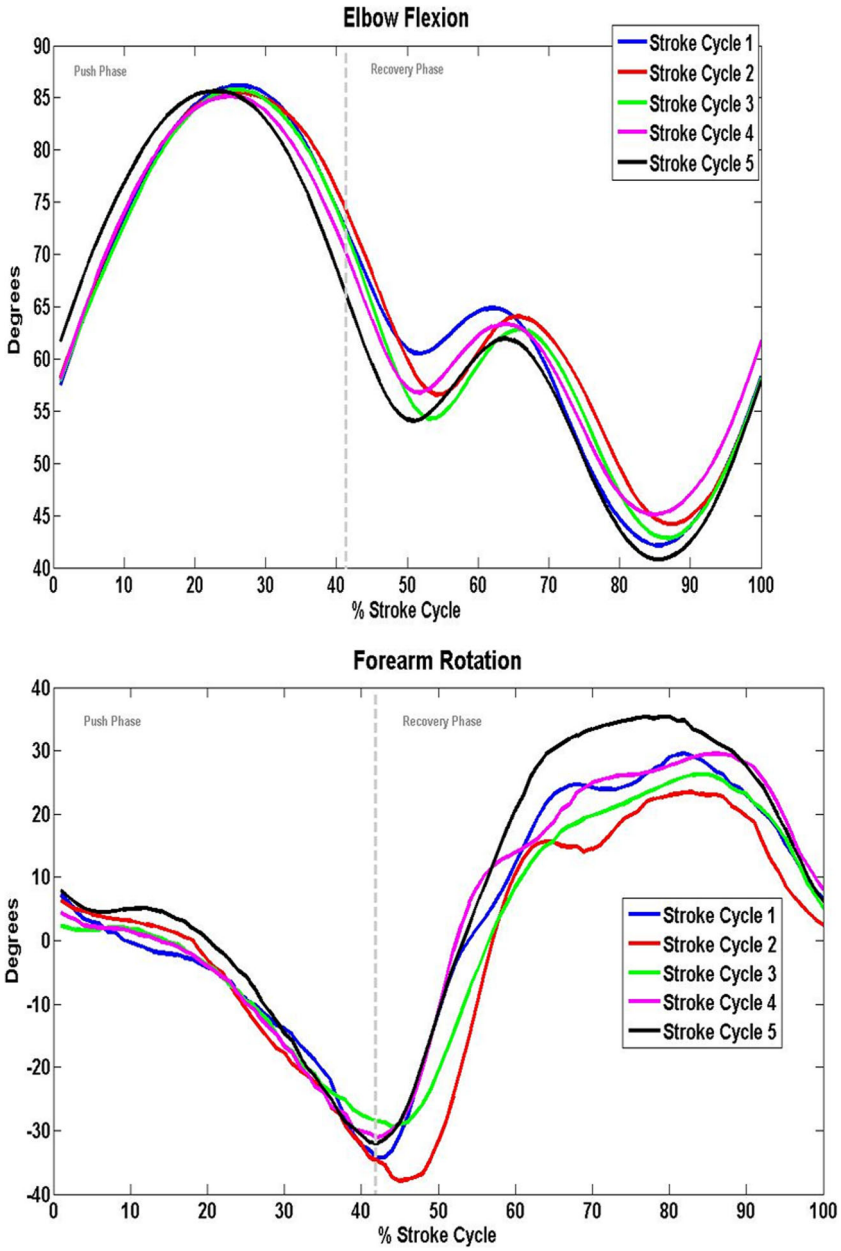


**Fig. 4** Kinematic profiles of the elbow generated by inverse kinematics simulations for all five stroke cycles. The profiles for elbow flexion are presented in the top panel, and the profiles for forearm rotation are presented in the bottom panel. The transition from push phase to recovery phase is indicated by the dotted line, in each panel. All angles are measured in degrees and are presented for 100% stroke cycle

peak moment responsible for shoulder rotation was also greater during the recovery phase (−2.9 Nm ± 0.4 Nm) than the push phase (−0.27 Nm ± 0.3 Nm). Peak shoulder rotation moment occurred during the recovery phase.

## 3.2 Muscle forces generated during wheelchair propulsion

An inverse dynamics-based approach was utilized to determine the muscle forces generated during wheelchair propulsion. The maximum muscle forces generated during the push phase of propulsion are displayed in Fig. 5. The muscles that generated the greatest average force over all five stroke cycles during the push phase (Fig. 5, top panel) were the serratus anterior (324.4 ± 21.4 N) and infraspinatus (269.6 ± 53.5 N). The subscapularis (180.5 ± 26.7 N), triceps (171.1 ± 10.6 N), middle deltoid (120.3 ± 20.0 N), posterior deltoid (73.7 ± 3.2 N), supraspinatus (53.4 ± 8.7 N), middle trapezius (22.5 ± 1.6 N), and biceps (21.9 ± 17.9 N) also contributed to push phase of propulsion. The pectoralis major (3.8 ± 0.004 N), anterior deltoid (1.5 ± 0.5 N), rhomboids major (1.3 ± 0.01 N), and upper trapezius (0 N), contributed little to no force to the push phase of wheelchair propulsion.

The maximum muscle forces generated during the recovery phase of propulsion are displayed in Fig. 5 (bottom panel). The muscles that generated the greatest

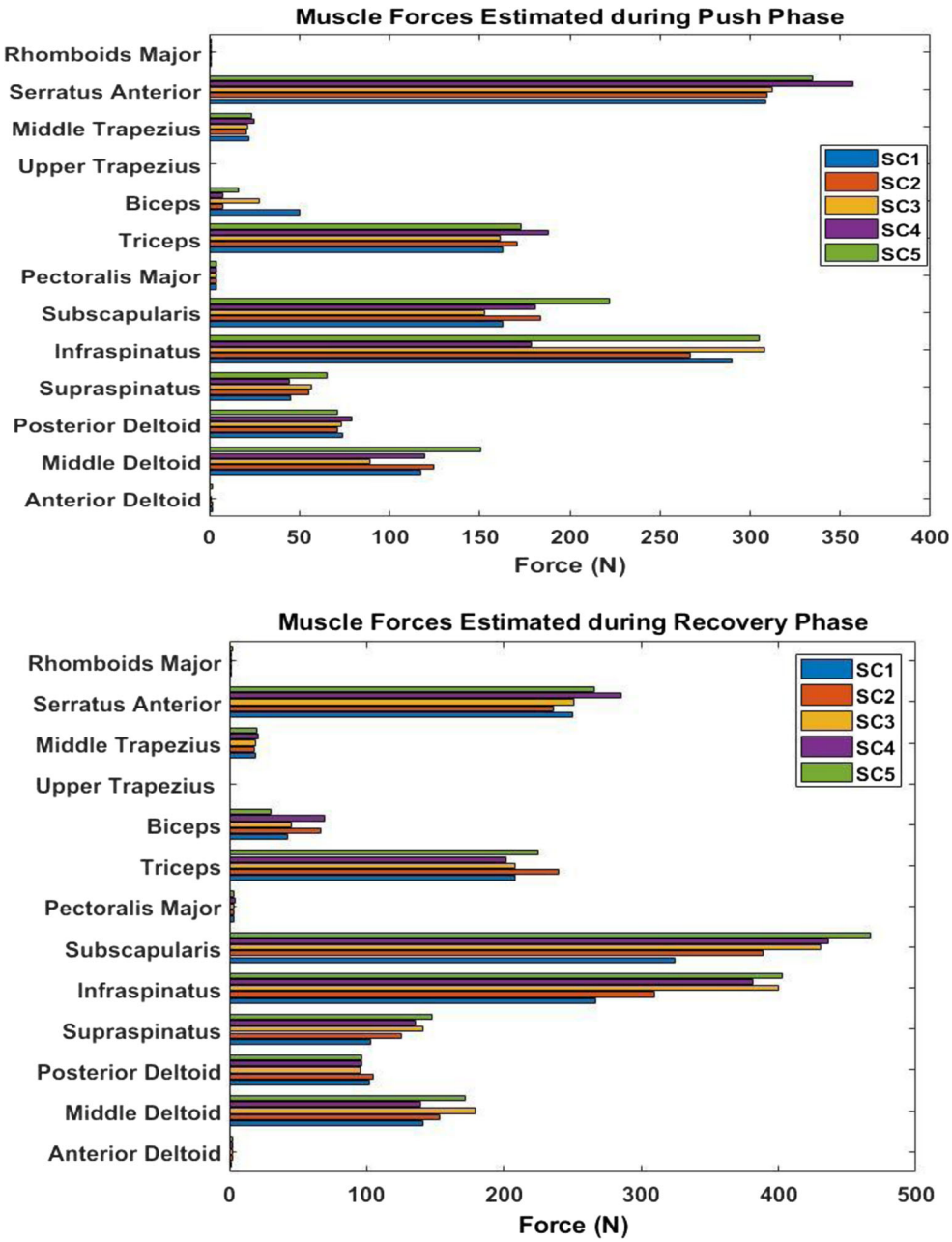


**Fig. 5** Maximum shoulder muscle forces estimated by static optimization for all five stroke cycles. Forces genereated during the push phase are presented in the top panel, while those generated during the recovery phase are presented in the bottom panel. All forces are presented in Newtons. The muscle forces for only the muscles for which experimental EMG was collected are presented in each panel

average force during the recovery phase (across all five stroke cycles) were the subscapularis (409.3 ± 54.9 N), and infraspinatus (352.0 ± 60.8 N). The serratus anterior (257.7 ± 18.7 N), triceps (216.5 ± 15.5 N), middle deltoid (156.9 ± 18.0 N), supraspinatus (130.6 ± 17.5 N), posterior deltoid (98.8 ± 4.3 N), biceps (50.6 ± 16.6 N), and middle trapezius (19.5 ± 1.4 N) also contributed to the recovery phase of propulsion. The pectoralis major (3.6 ± 0.1 N), anterior deltoid (2.3 ± 0.4 N), rhomboids major (1.5 ± 0.2 N), and upper trapezius (0 N) generated little to no force during the recovery phase.

### 3.3 Mean absolute error analysis

For a quantitative analysis, the *MAE* was calculated for each muscle during each stroke cycle (Table 2). On average, the muscles that demonstrated excellent correlation (0.05–0.09) are middle deltoid, supraspinatus, infraspinatus, subscapularis, biceps, and serratus anterior. On average, the posterior deltoid demonstrated good correlation (0.20). The muscles that demonstrated poor correlation (0.27–0.40) are anterior deltoid, triceps, and rhomboid major. All three muscles consistently had a poor correlation over each stroke cycle. The muscle with the

**Table 2** Mean absolute error (*MAE*) per stroke cycle. *MAE* values in italics have an excellent to good correlation

| Muscle | Stroke Cycle 1 | Stroke Cycle 2 | Stroke Cycle 3 | Stroke Cycle 4 | Stroke Cycle 5 | Average |
|---|---|---|---|---|---|---|
| Anterior deltoid | 0.50 | 0.47 | 0.35 | 0.33 | 0.34 | 0.40 ± 0.08 |
| Middle deltoid | *0.08* | *0.08* | *0.08* | *0.10* | *0.09* | *0.09 ± 0.01* |
| Posterior deltoid | *0.19* | *0.18* | 0.21 | 0.21 | *0.20* | *0.20 ± 0.01* |
| Supraspinatus | *0.06* | *0.05* | *0.05* | *0.06* | *0.05* | *0.05 ± 0.01* |
| Infraspinatus | *0.07* | *0.07* | *0.07* | *0.07* | *0.07* | *0.07 ± 0* |
| Subscapularis | *0.05* | *0.06* | *0.07* | *0.06* | *0.07* | *0.06 ± 0.01* |
| Tricep | 0.31 | 0.33 | 0.29 | 0.30 | 0.31 | 0.31 ± 0.01 |
| Bicep | *0.08* | *0.05* | *0.06* | *0.04* | *0.06* | *0.06 ± 0.01* |
| Serratus anterior | *0.08* | *0.08* | *0.08* | *0.07* | *0.07* | *0.08 ± 0.01* |
| Rhomboid major | 0.27 | 0.27 | 0.27 | 0.30 | 0.26 | 0.27 ± 0.02 |
| Average | *0.17 ± 0.15* | *0.16 ± 0.15* | *0.15 ± 0.11* | *0.15 ± 0.12* | *0.15 ± 0.11* | *0.16 ± 0.13* |

best average correlation is the supraspinatus (0.05). Considering all ten muscles across all five stroke cycles, the average correlation was good (0.16).

## 4 Discussion

The two objectives of this study were to (i) construct a dynamic, patient-specific model of the upper limb and trunk and (ii) establish proof of concept by evaluating the model with data obtained from a manual wheelchair user with tetraplegia. This study builds upon previous wheelchair propulsion simulation studies by providing a new model of the trunk and upper limb that contains the deep and superficial muscles of the shoulder complex. Kinematically, the model is consistent with the Stanford VA Model [25]. The presented model was evaluated using data collected from a manual wheelchair user with tetraplegia, since they are at a greater risk for shoulder pain and injury. Manual wheelchair user populations used to evaluated previous patient-specific models were either individuals with paraplegia or a heterogeneous group of manual wheelchair users. The kinematic profiles generated from the inverse kinematics simulations with our model are consistent with those generated by other studies [27]. This is also the first study to incorporate fine-wire EMG data collected from the study subject. The model was evaluated quantitatively by computing the *MAE*. This analysis addressed the error in the muscle activation magnitude estimated by the model and was a surrogate for validating the model estimation of muscle force [12, 24, 43].

Good correlations for *MAE* of estimated muscle activation and experimental EMG were observed for seven of the ten of the muscles for each stroke cycle, while the remaining three muscles had poor correlations. The results of the *MAE* calculations were highly consistent across all stroke cycles and the mean *MAE* s across all stroke cycles concur with previous studies [12, 24]. Of the ten muscles investigated, the rhomboid major, triceps, and anterior deltoid muscles consistently had poor correlations for each stroke cycle. These cases are indicative of lack of a relationship between the muscle activation determined by the model and the experimental EMG. The high *MAE* calculated for the rhomboid major may be due to the limited scapula motion, defined by the model prohibiting scapular retraction. The scapula could not move in isolation, as mentioned previously [25]. When comparing the muscle activation profile with the experimental EMG profile, no similarities between the two exist, further confirming that the model did not capture scapular retraction.

The triceps had a high *MAE*, indicative of a poor correlation for all stroke cycles. Dubowsky et al. [12] also observed poor *MAE* values for the triceps muscle in a participant with paraplegia. Furthermore, they observed that the duration of experimental triceps activity was much longer than that which was calculated computationally. Since their participant was tested for full upper limb function, the authors suggested that the lack of parity between computational and experimental results may be due to the participant using his triceps in a compensatory manner as a result of limited trunk control. They postulated that future work with fine-wire EMG investigating other prominent muscles in wheelchair propulsion, such as the muscles of the rotator cuff, may shed light on the contraction/co-contraction results [12]. Fine-wire EMG was utilized with the current study. Based on the experimental EMG profile of the participant in this study, the triceps was most active between 20 and 70% of the stroke cycle, as displayed in Fig. 6. However, the computational results suggest that the muscle force was generated between 10 and 80% of the stroke cycle. The rotator cuff muscles

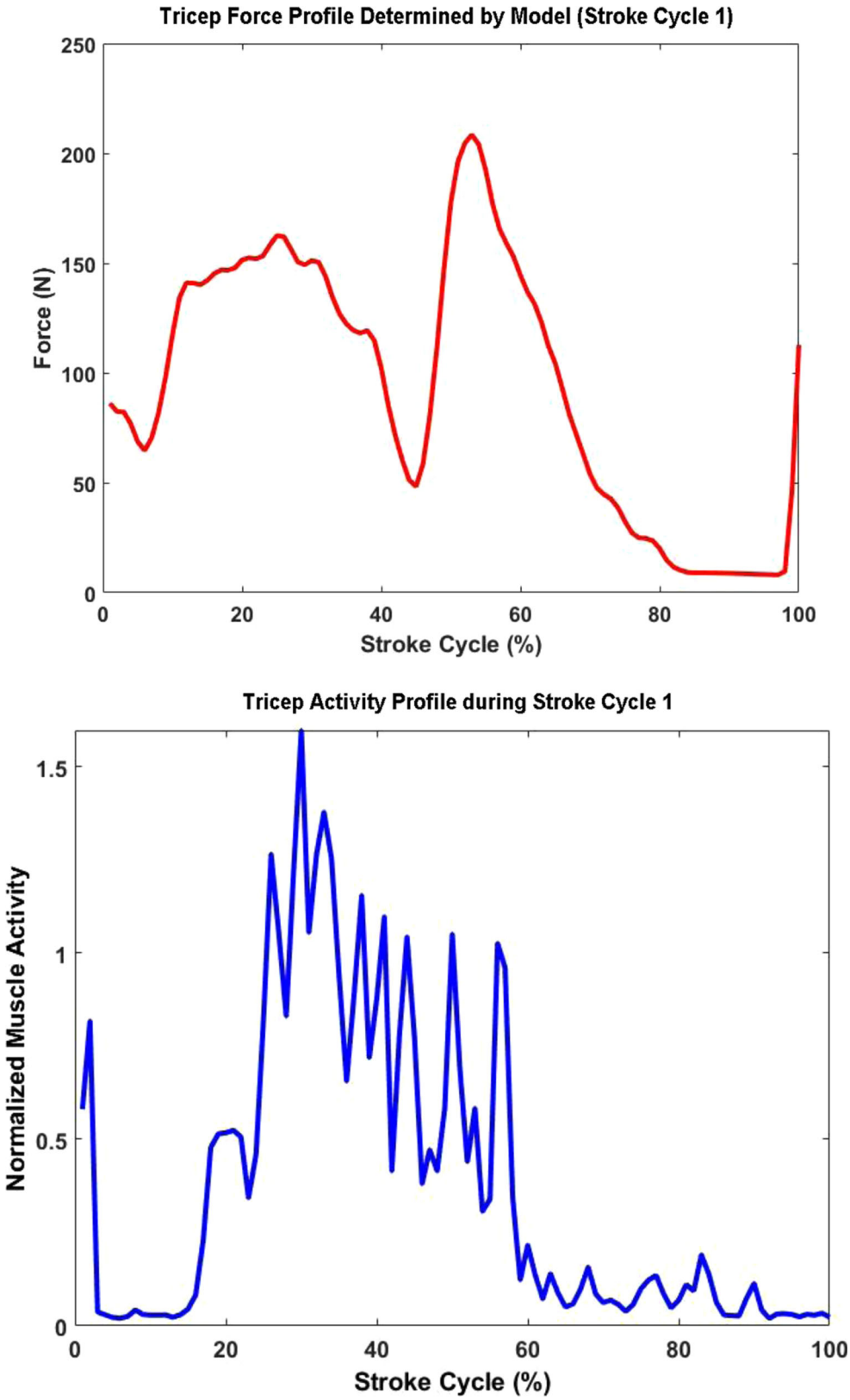


**Fig. 6** Triceps force profile computed for 100% stroke cycle (top panel) and experimental triceps EMG profile during 100% stroke cycle (bottom panel). The computed force profile demonstrates triceps activity for about 10–80% of the stroke cycle. However, the experimental EMG profile demonstrates triceps activity for 20–70% of the stroke cycle

investigated (infraspinatus, supraspinatus, subscapularis) all had excellent *MAE* values, so it is less likely that the lack of parity between computational and experimental results is due to compensatory use of the triceps.

Morrow et al. [24] did not report poor *MAE* values for the triceps. For model validation, they selected three optimal criteria for the determination of the cost function used in the static optimization technique: (i) linear minimization of $\alpha$, muscle activation [44]; (ii) minimax formulation of minimizing the maximum muscle stress [45]; and (iii) nonlinear minimization of the sum of muscle stress cubed [39]. Their study population consisted of 11 manual wheelchair using individuals with paraplegia and one with spina bifida. They reported an average *MAE* value for each muscle and criterion investigated and specifically reported excellent average *MAE* value for the triceps for each criterion. The objective function selected in this current study was minimization of muscle activation squared [15], whereas the objective function selected by Dubowsky et al. [12] was minimization of muscle effort. The difference in the objective function may be more of a determinant for the tricep *MAE*. This suggests that the poor *MAE* values reported for the triceps may be due to the objective function selected.

The anterior deltoid had the highest *MAE* of all of the muscles investigated across all five stroke cycles. Compared to previous studies, Dubowsky et al. [12] observed good *MAE* values for the anterior deltoid muscle in a participant with paraplegia and an able-bodied participant. They observed an excellent *MAE* value in another participant with paraplegia. Morrow et al. [24] reported a good average *MAE* value for the anterior deltoid for each criterion; however, the standard deviations for the anterior deltoid were the highest for all of the muscles they investigated (linear $0.15 \pm 0.16$, minimax stress $0.12 \pm 0.09$, nonlinear $0.14 \pm 0.14$). The standard deviations and the MAEs had high variability compared to the means, which may have been reflective of the objective function implemented. This further supports the idea that the poor *MAE* values may be due to the objective function selected. At the very least, future work should investigate different objective functions for the selection of an optimal cost function for static optimization. Also, these objective functions will also be evaluated for their suitability in other applications, such as reaching and FES control. Furthermore, the muscles investigated should be validated with *MAE* in conjunction with fine-wire EMG.

There are a number of limitations to the study. A significant limitation of this study is the sample size. The model evaluation was designed as a proof-of-concept study, so only one participant was investigated. The findings presented from the patient-specific model are indicative of the participant studied and may not necessarily be indicative of all manual wheelchair users with tetraplegia. However, other computer graphics-based models have been evaluated and validated successfully with one study participant [26, 43]. At a minimum, the presented results are encouraging to conduct a future study with a larger cohort of individuals with tetraplegia.

The Wheelchair Propulsion Model is based on the OpenSim Arm 26 Model, and its upper limb kinematics is consistent with the Stanford VA Model [25]. Therefore, the limitations in shoulder movement previously discussed for the Stanford VA Model are also limitations in the Wheelchair Propulsion Model. Specifically, the motion of the scapula and clavicle were constrained to depend on the motion of the humerus, so the motion of the shoulder girdle is very simplified. The motions of the scapula and humerus vary only with humeral elevation. The limited scapular motion may have affected the muscle force estimates for the muscles responsible for scapular motion, such as the rhomboid major.

The muscle parameters in the model for optimal force, muscle length, and tendon slack length were all obtained from cadaver studies. The parameters included for the serratus anterior and the rhomboid major were estimated from Garner and Pandy's [33] upper limb model. There were no values for these muscles in the literature, and the authors noted that their model overestimated muscle parameters for the upper limb muscles. It is possible that the parameters for the serratus anterior included in the model are overestimated.

A limitation of static optimization is it is performed per frame (quasi-static), even though the motions analyzed are dynamic [24]. Manual muscle test data were not available for the triceps and other muscles of the shoulder complex, so partial muscle paralysis due to SCI was not considered in the model. These data would have informed an appropriate estimate of the increase or decrease of the optimal forces on the muscles [16] to account for deficits due to SCI. Also, in order to successfully use the static optimization approach, extra actuators were appended to the coordinates in the model so that the joints could achieve the computed acceleration for each time point. Static optimization attempts to solve the redundancy problem for actuators and muscles by using the accelerations computed from the ID solution as a constraint [13, 43]. When the muscles in a model are weak, coordinate actuators can be appended to joints in the model. The amount of actuation needed at a given joint can be determined and the muscles can be strengthened accordingly. However, we determined that the actuators had a negligible contribution to the estimated muscle forces, as they were less than 5% of the net joint moments [23]. Moreover, the static optimization technique has been successfully used in previous studies [12, 24], while Rankin et al. [26, 27] used the dynamic optimization approach. Recently, Morrow et al. [46] compared muscle forces predicted by static and dynamic optimization during wheelchair propulsion. Investigating the push phase of wheelchair propulsion, they determined that the muscle forces generated by static optimization adequately produced the motion and joint moments at the shoulder. However, they noted deviations in the elbow moment, pronation-supination movement, and hand rim forces. Therefore, they suggested that static optimization does not produce results similar enough to be used as an alternative to dynamic optimization. They also suggested that dynamic optimization may be required for motions that are greatly influenced by muscle activation dynamics or that require significant co-contraction, as the static optimization may be underestimating the co-

contraction. After reviewing the raw EMG data for the participant in our study, we found co-contraction among the muscles, especially the infraspinatus and the middle deltoid. However, the mean *MAE* for each stroke cycle demonstrated a good correlation between the estimated muscle activation and the experimental EMG. Considering the observances of good correlations between most of the muscles investigated, the good correlation for the overall mean *MAE*, and the subject propelled in his own chair at a slow speed (2 mph), we believe that our use of the static optimization approach was appropriate. While this proof-of-concept evaluation was conducted on one subject, we plan to evaluate the model with additional subjects. The raw EMG data will be reviewed for evidence of significant co-contraction before evaluation with the model, and if present, we may consider utilizing a dynamic optimization approach.

The optimal forces of the muscles in the model used in this study were obtained from published cadaver studies [47], with the exception of the serratus anterior and the rhomboid major (obtained from [33]). Given the accelerations generated from the inverse dynamics simulations, the static optimization simulations would not converge unless actuators were appended to the model. Therefore, the optimal forces (based on cadaver-based estimates for segment mass and moment of inertia and meant for use with able-bodied populations) may not have been adequate for the participant with tetraplegia investigated. To address these concerns, future work should investigate force-tension-length curves that are more reflective of individuals with SCI.

Finally, evaluation of the model with experimental EMG was greatly affected by the sensitivity of EMG timing of activation. The experimental data were originally collected to investigate the biomechanical predictors shoulder pain in manual wheelchair users with tetraplegia [35]. Thus far, EMG analyses from the original work have determined the level of muscle activation (amplitude and phasing) relative to the kinematics during the push cycle [35]. Since these data were not collected with the intention of being incorporated in a patient-specific model, the precision of EMG onset and offset times received very little attention. Therefore, it is possible that this lack of precision or sensitivity could have affected the results. Future work should include the development of EMG algorithms that more clearly identify the onset and offset times, followed by the recalculation of the MAEs.

## 5 Conclusions

The two objectives of this study were to (i) construct a dynamic, patient-specific model of the upper limb and trunk and (ii) establish proof of concept by evaluating the model with data obtained from a manual wheelchair user with tetraplegia. The Wheelchair Propulsion Model, constructed using OpenSim, contains shoulder and trunk muscles that have been commonly investigated in wheelchair propulsion biomechanics studies. The novelty of this model is that is also contains the following muscles that play a role in wheelchair propulsion and have not been included in previous models: upper and middle trapezius, serratus anterior, and rhomboid major. The model is kinematically consistent with previous models. To establish proof of concept, the model was evaluated with kinematic and kinetic data obtained from a manual wheelchair user with tetraplegia. The significance is that these individuals are at a greater risk for shoulder pain and injury, but have not been included in previous wheelchair propulsion simulation studies. Using the subject's data, a patient-specific model was generated. The shoulder profiles generated from the inverse kinematics simulations were consistent with previous studies of manual wheelchair users.

An inverse dynamics-based approach was implemented to determine the individual shoulder muscle contribution to manual wheelchair propulsion. This is the first study to evaluate muscle forces with fine-wire EMG collected on the individual being investigated, as previous studies only utilized surface EMG [12, 27, 39]. The significance of collecting the fine-wire EMG is to record the activity of the deep shoulder complex musculature, as it may provide further insight to joint coupling [25]. Model evaluation was achieved by calculating the *MAE* of the estimated activation and the fine-wire EMG. The overall *MAE* for each stroke cycle demonstrated a good correlation between the simulated muscle activations and the experimental muscle activity, demonstrating the model's ability to estimate muscle forces during wheelchair propulsion. Having established proof of concept, future work will evaluate the model with a larger cohort of manual wheelchair users with tetraplegia as well as conduct studies to optimize wheelchair propulsion. To encourage other wheelchair biomechanists to participate in the OpenSim community, the Wheelchair Propulsion Model will be freely accessible. This will allow other researchers to access the model to replicate our results, make alterations to the model to address their specific research problems, and contribute to the advancement of wheelchair propulsion biomechanics.

**Acknowledgments** The authors thank Mr. Andrew Kwarciak and Dr. Mathew Yarossi for collecting and processing the experimental wheelchair propulsion and EMG data that were used in the simulations.

**Funding** This study was funded by NJCSCR Grant No. 06-3054-SCR-E-0 and NSF/CUNY Grant No. 0450360.

## References

1. Consortium for Spinal Cord Medicine (2005) Preservation of upper limb function following spinal cord injury: a clinical practice guideline for health-care professionals. J Spinal Cord Med 28:433–470
2. Dyson-Hudson TA, Kirshblum SC (2004) Shoulder pain in chronic spinal cord injury, part I: epidemiology, etiology, and pathomechanics. J Spinal Cord Med 27:4–17
3. Sie IH, Waters RL, Adkins RH, Gellman H (1992) Upper extremity pain the postrehabilitation spinal cord injured patient. Arch Phys Med Rehabil 73:44–48

4. Curtis KA, Tyner TM, Zachary L, Lentell G, Brink D, Didyk T, … Pacillas B (1999) Effect of a standard exercise protocol on shoulder pain in long-term wheelchair users. Spinal Cord 37(6):421–429
5. Curtis KA, Drysdale GA, Lanza RD, Kolber M, Vitolo RS, West R (1999) Shoulder pain in wheelchair users with tetraplegia and paraplegia. Arch Phys Med Rehabil 80:453–457
6. Kulig K, Rao SS, Mulroy SJ, Newsam CJ, Gronley JK, Bontrager EL, Perry J (1998) Shoulder joint kinetics during the push phase of wheelchair propulsion. Clin Orthop Relat Res 354:132–143
7. Mulroy SJ, Gronley JK, Newsam CJ, Perry J (1996) Electromyographic activity of shoulder muscles during wheelchair propulsion by paraplegic persons. Arch Phys Med Rehabil 77(2):187–193
8. Powers CM, Newsam CJ, Gronley JK, Fontaine CA, Perry J (1994) Isometric shoulder torque in subjects with spinal cord injury. Arch Phys Med Rehabil 75:761–765
9. Reyes ML, Gronley JK, Newsam CJ, Mulroy SJ, Perry J (1995) Electromyographic analysis of shoulder muscles of men with low-level paraplegia during a weight relief raise. Arch Phys Med Rehabil 76:433–439
10. Dubowsky SR, Sisto SA, Langrana NA (2009) Comparison of kinematics, kinetics, and EMG throughout wheelchair propulsion in able-bodied and persons with paraplegia: an integrative approach. J Biomech Eng 131(2):021015
11. Correa TA, Baker R, Graham HK, Pandy MG (2011) Accuracy of generic musculoskeletal models in predicting the functional roles of muscles in human gait. J Biomech 44:2096–2105
12. Dubowsky SR, Rasmussen J, Sisto SA, Langrana NA (2008) Validation of a musculoskeletal model of wheelchair propulsion and its application to minimizing shoulder joint forces. J Biomech 41(14):2981–2988
13. Erdemir A, McLean S, Herzog W, van der Bogert AJ (2007) Model-based estimation of muscle forces exerted during movements. Clin Biomech 22:131–154
14. Nikooyan AA, Veeger HEJ, Westerhoof P, Graichen F, Bergmann G, van der Helm FCT (2010) Validation of the Delft shoulder and elbow model using in-vivo glenohumeral joint contact forces. J Biomech 43:3007–3014
15. van der Helm FCT (1994) A finite element musculoskeletal model of the shoulder mechanism. J Biomech 27:551–569
16. van Drongelen S, van der Woude LH, Janssen TW, Angenot EL, Chadwick EK, Veeger DJH (2005) Glenohumeral contact forces and muscle forces evaluated in wheelchair-related activities of daily living in able-bodied subjects versus subjects with paraplegia and tetraplegia. Arch Phys Med Rehabil 86:1434–1440
17. van Drongelen S, van der Woude LH, Janssen TW, Angenot EL, Chadwick EK, Veeger DH (2005) Mechanical load on the upper extremity during wheelchair activities. Arch Phys Med Rehabil 86(6):1214–1220
18. van Drongelen S, van der Woude LH, Veeger HE (2011) Load on the shoulder complex during wheelchair propulsion and weight relief lifting. Clin Biomech 26(5):452–457
19. Veeger HE, Rozendaal LA, van der Helm FC (2002) Load on the shoulder in low intensity wheelchair propulsion. Clin Biomech 17(3):211–218
20. Fregly BJ, Boninger ML, Reinkensmeyer DL (2012) Personalized neuromusculoskeletal modeling to improve treatment of mobility impairments: a perspective from European research sites. JNER 9:18. https://doi.org/10.1186/1743-0003-9-18
21. Delp SL, Anderson FC, Arnold AS, Loan P, Habib A, John CT, … Thelen DG (2007) OpenSim: open-source software to create and analyze dynamic simulations of movement. IEEE Trans Biomed Eng 54(11):1940–1949
22. Saul KR, Hu X, Goehler CM, Vidt ME, Daly M, Velisar A, Murray M (2014) Benchmarking of dynamic simulation predictions in two software platforms using an upper limb musculoskeletal model. CMBBE 18(13):1445–1458
23. Hicks JL, Uchida TK, Seth A, Rajagopal A, Delp SL (2015) Is my model good enough? Best practices for verification and validation of musculoskeletal models and simulations of movement. J Biomech Eng 137(2):0209505–020905-24. https://doi.org/10.1115/1.4029304
24. Morrow MMB, Kaufman KR, An KN (2010) Shoulder model validation and joint contact forces during wheelchair activities. J Biomech 43:2487–2492
25. Holzbaur KR, Murray WM, Delp SL (2005) A model of the upper extremity for simulating musculoskeletal surgery and analyzing neuromuscular control. Ann Biomed Eng 33(6):829–840
26. Rankin JW, Kwarciak AM, Richter WM, Neptune RR (2010) The influence of altering push force effectiveness on upper extremity demand during wheelchair propulsion. J Biomech 43:2771–2779
27. Rankin JW, Richter WM, Neptune RR (2011) Individual muscle contributions to push and recovery subtasks during wheelchair propulsion. J Biomech 44:1246–1252
28. Mulroy SJ, Farrokhi S, Newsam CJ, Perry J (2004) Effects of spinal cord injury level on the activity of shoulder muscles during wheelchair propulsion: an electromyographic study. Arch Phys Med Rehabil 85:925–934
29. Seth A, Sherman M, Reinbolt JA, Delp SL (2011) OpenSim: a musculoskeletal modeling and simulation framework for in silico investigations and exchange. 2011 symposium on human body dynamics. Procedia IUTAM 2:212–232
30. Odle BM, Forrest GF, Reinbolt J, Dyson-Hudson TA (2011) Development of an OpenSim shoulder model for manual wheelchair users with tetraplegia. Proceedings of the ASME 2011 International Mechanical Engineering Congress & Exposition, Denver, CO, November 11–17
31. Winter DA (2005) Biomechanics and motor control of human movement, 3rd edn. Wiley, Hoboken
32. Vasavda AN, Li S, Delp SL (1998) Influence of muscle morphometry and moment arms on the moment-generating capacity of human neck muscles. Spine 24(4):412–422
33. Garner BA, Pandy MG (2003) Estimation of musculotendon properties in the human upper limb. Ann Biomed Eng 31:207–220
34. Zajac FE (1989) Muscle and tendon: properties, models, scaling, and application to biomechanics and motor control. Crit Rev Biomed Eng 17(4):359–411
35. Yarossi M, Dyson-Hudson TA, Forrest G, Kwarciak A, Sisto SA (2010) Shoulder kinematics and kinetics during wheelchair propulsion in persons with tetraplegia. Proceedings of the American Society of Biomechanics. Providence, RI, August 18–21
36. Kirshblum SC, Burns SP, Biering-Sorensen F, Donovan W, Graves DE, Jha A, … Waring W (2011) International standards for neurological classification of spinal cord injury (revised 2011). JSCM 34(6):535–546
37. Wu G, van der Helm FCT, Veeger HEJ, Makhsous M, Van Roy P, Anglin C, … Buchholz B (2005) ISB recommendation on definitions of joint coordinate systems of various joints for reporting of human joint motion- part II: shoulder, elbow, wrist, and hand. J Biomech 38:981–992
38. Crowninshield RD (1978) Use of optimization techniques to predict muscle forces. J Biomech Eng 100:88–92
39. Lin HT, Su FC, Wu HW, An KN (2004) Muscle force analysis in the shoulder mechanism during wheelchair propulsion. Proc Inst Mech Eng H J Eng Med 218:213–221
40. Hof AL (1997) The relationship between electromyogram and muscle force. Sportverletz Sportschaden 11(3):79–86
41. Cereatti A, Della Croce U, Cappozzo A (2006) Reconstruction of skeletal movement using skin markers: Comparative assessment of bone pose estimators. JNER 3:7. https://doi.org/10.1186/1743-0003-3-7
42. Chiari L, Della Croce U, Leardini A, Cappozzo A (2005) Human movement analysis using stereophotogrammetry part 2: instrumental errors. Gait Posture 21:197–211

43. de Zee M, Dalstra M, Cattaneo PM, Rasmussen J, Svensson P, Melsen B (2007) Validation of a musculo-skeletal model of the mandible and its application to the mandibular distraction osteogenesis. J Biomech 40:1192–1201
44. Kaufman KR, An KN, Litchy WJ, Chao EYS (1991) Physiological prediction of muscle forces: II. Application to isokinetic exercise. Neuroscience 40:793–804
45. An KN, Kwak BW, Chao EY, Morrey BF (1984) Determination of muscle and joint forces: a new technique to solve the indeterminate problem. J Biomech Eng 106:364–367
46. Morrow MM, Rankin JW, Neptune RR, Kaufman KR (2014) A comparison of static and dynamic optimization muscle force predictions during wheelchair propulsion. J Biomech 47:3459–3465
47. Dempster WT (1955) Space requirements of the seated operator. WADC. Technical Report (TR-55-159). Wright-Patterson Air Force Base, OH


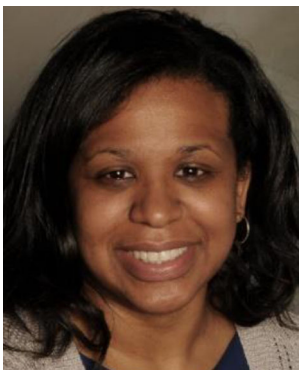

**Brooke Odle** received the B.S. degree in bioengineering from the University of Pittsburgh, Pittsburgh, PA, and the M.S. degree in biomedical engineering from New Jersey Institute of Technology, Newark, NJ, as well as the doctorate in biomedical engineering from New Jersey Institute of Technology and Rutgers University Biomedical and Health Science, Newark, NJ (Joint Program in Biomedical Engineering). She is currently working as a Postdoctoral Fellow in the Department of Biomedical Engineering at Case Western Reserve University, Cleveland, OH. Her research interests include biomechanics of human movement, rehabilitation engineering, computational musculoskeletal modeling, and motor control.

**Jeffrey Reinbolt** , Ph. D., is an Associate Professor in the Department of Mechanical, Aerospace, and Biomedical Engineering at the University of Tennessee-Knoxville. Dr. Reinbolt's research interests include the development of computational tools and their application to complex biodynamic systems, forward dynamics simulation-based treatment planning, patient-specific modeling, inverse dynamics simulations to predict novel movements, optimization techniques, and surgical robots for minimally invasive surgery.

**Gail F Forrest** , Ph.D., Associate Director of Human Performance and Engineering Research at Kessler Foundation, is also Assistant Professor, Department of Physical Medicine and Rehabilitation at Rutgers – New Jersey Medical School. Dr. Forrest's research interests include neuroplasticity, improvement in secondary consequences and restoration of function for individuals after spinal cord injury. Other key interests are in the area of biomechanics as related to modeling algorithms for understanding control mechanisms in upper extremity (i.e., arm reaching after stroke), and postural control during locomotion. All her areas of research are ultimately focused toward the improvement of functional mobility. Currently, she is combining exoskeletal-assisted walking with external electrical stimulation of the spinal cord toward potentially promoting voluntary muscle firing and independent walking.

**Trevor A. Dyson-Hudson** , M.D. is the Director of the Spinal Cord Injury Research and Outcomes & Assessment Research at Kessler Foundation and Project Co-Director of the Northern New Jersey Spinal Cord Injury System (NNJSCIS)—a NIDILRR-funded Spinal Cord Injury Model System of care. He is an Associate Professor in the Department of Physical Medicine and Rehabilitation (PM&R) at Rutgers New Jersey Medical School and a Member of the Graduate Faculty at Rutgers Graduate School of Biomedical Sciences. Dr. Dyson-Hudson's research interests include preservation and restoration of function and mobility in persons with SCI and the prevention and treatment of common secondary medical complications affecting this population. Dr. Dyson-Hudson holds committee appointments in the American Spinal Injury Association (ASIA) and the American Paraplegia Society (APS)/Academy of Spinal Cord Injury Professionals (ASCIP) and is on the APS Board of Directors.